Crystalline structures of l-cysteine and l-cystine: a combined theoretical and experimental characterization

Yangyang Su, Etienne Hessou, Estefania Colombo, Gustavo Belletti, Ali Moussadik, Ivan T. Lucas, Vincent Frochot, Michel Daudon, Stéphan Rouzière, Dominique Bazin, et al.

Crystalline Structures of L-Cysteine and L-Cystine; A Combined Theoretical and Experimental Characterization

Yangyang Su[1,2], Etienne P. Hessou[1], Estefania Colombo[3], Gustavo Belletti[3], Ali Moussadik[1], Ivan Lucas[4], Vincent Frochot[5,6], Michel Daudon[5,6], Stephan Rouziere[7], Dominique Bazin[8], Kezhi Li[2], Paola Quaino[3], and Frederik Tielens[1,*]

[1]General Chemistry (ALGC), Materials Modeling Group, Vrije Universiteit Brussel (Free University Brussels-VUB), Pleinlaan 2, 1050 Brussel, Belgium

[2]State Key Laboratory of Solidification Processing, Shaanxi Key Laboratory of Fiber Reinforced Light Composite Materials, Northwestern Polytechnical University, Xi'an 710072, China

[3]IQAL, Instituto de Química Aplicada del Litoral, CONICET-UNL, 3000 Santa Fe, Argentina

[4] Laboratoire LISE UMR 8235 CNRS-SU, Sorbonne Université, Paris, France

[5]UMR S1155, INSERM/UPMC, 4 Rue de la Chine, 75970 Paris Cedex 20, France

[6]AP - HP, Hôpital Tenon, Explorations Fonctionnelles Multidisciplinaires, 4 Rue de la Chine, 75970 Paris Cedex 20, France

[7]Université Paris-Saclay, CNRS, Laboratoire de Physique des Solides, 91405, Orsay, France

[8]Institut de Chimie Physique, Université Paris Sud, 310, rue Michel Magat, 91400 Orsay, France

* Author to whom correspondence should be sent. frederik.tielens@vub.be

Abstract

It is assumed that genetic diseases affecting the metabolism of cysteine and the kidney function lead to two different kinds of pathologies, namely cystinuria and cystinosis whereby generate L-cystine crystals. Recently, the presence of L-cysteine crystal has been underlined in the case of cystinosis. Interestingly, it can be strikingly seen that cystine ([-S-CH_2-CH-(NH_2)-COOH]$_2$) consists of two cysteine ($C_3H_7NO_2S$) molecules connected by a disulfide (S-S) bond. Therefore, the study of cystine and cysteine is important for providing a better understanding of cystinuria and cystinosis. In this paper, we elucidate the discrepancy between L-cystine and L-cysteine by investigating the theoretical and experimental infrared spectra (IR), X-ray diffraction (XRD) as well as Raman spectra aiming to obtain a better characterization of abnormal deposits related to these two genetic pathologies.

Keywords: A1. Biominerals; A1. Computer simulations; A.1. Crystal structure; A1. Characterization; B1. L-cysteine; B1. L-cystine

1. Introduction

Kidney stone formation, also known as nephrolithiasis is the result of an imbalance between supersaturated solutes and crystallization inhibitors in urine.[1-4] More precisely, the low solubility of L-cystine (about 240 mg/L in urine) may explain its crystallization in the nephrons and formation of kidney stones observed in patients with cystinuria. Due to its very high water solubility (about 280 g/L), L-cysteine crystal may not form in body fluids or urine, but L-cystine and/or L-cysteine may accumulate within lysosome cells in patients suffering from a rare inherited disease named cystinosis which results from mutations of CTNS gene.[5]

The prevalence and incidence of kidney stones has increased over the past 30 years and this for reasons that remain incompletely understood.[6-8] Cystinuria is the most common genetic renal disease that induces nephrolithiasis with a prevalence less than 1:7000 births in an average worldwide depending on the population (1/2500 among Lebanese Jews, 1/5000 among Americans, 1/18,000 among Japanese, 1/20,000 among France and 1/100,000 among Swedish). In Europe, cystinuria accounts for 1% ~ 2% of all kidney stones.[9, 10] Although the amount of cystinuria patients is smaller than that of calcium oxalate or hydroxyapatite stone formers, the formation of such cystinuria is also a very active and multi-recurrent stone disease,[11, 12] with a high risk of chronic kidney disease.[13] An important inconvenience is that extracorporeal shockwave lithotripsy is often ineffective because of the relative elasticity of cystine stones, which makes it insensible to shock wave-treatment. Thus, open surgery is too often the only answer, especially in developing countries, in affected patients with large and/or multiple stones, which is very common.

Nowadays, in many cases, percutaneous nephrolithotomy and flexible ureteroscopy are chosen to treat cystine stones. Additionally, the treatment option with lasers is also efficient alternative in terms of destroying such stones. As is the case in other types of stones, the treatment methods rely on the size, location and crystal habits of the stones. However, some controversies still exist on which method should be selected between simple monitoring and urological intervention. The growth of the stone is difficult to stop if it is not expelled. Thus, it is encouraged to release the excretory cavities as soon as possible to hinder the recurrence.

Regarding cystinuria, it seems that L-cystine crystals are the main reason of the clinical pathology. As reported by Bazin et al.,[14] medical treatment may alter cystine crystals. These authors find that alkalinization with sodium bicarbonate can influence the crystal size of cystine as observed by means of powder neutron diffraction. Other treatments with molecules that contain S-H groups may alter the stone structure as shown by scanning electron microscopy examination.[14] These results could provide arguments for studying relationships between drugs

and formation of cystine stone. Therefore, it could be clinically relevant to investigate further the cystine structure in order to improve cystinuria and/or cystinosis treatment. Combined with real-time in situ atomic force microscopy, Rimer's work[15] reveals that L-cystine dimethyl ester and L-cystine methyl ester obviously inhibit the cystine crystal growth of the {100} face which reduces the aggregation of cystine crystallites. In Rimer's report,[15] it has been indicated L-cysteine can reduce the crystal size of L-cystine, but does not change the crystallization yield of L-cystine, thus showing the inability of such L-cysteine in the prevention of L-cystine' growth in kidney stones.

Normally, urine contains two components, i.e., L-cysteine and L-cystine at a neutral pH, L-cysteine can be partially oxidized to L-cystine.[16, 17] Dewey et al.[18] report the conversion between cysteine and cystine through evaluating different concentrations in precursor solution under irradiating condition and how these environments impact the S-H and S-S bonds. This is like the conversion between di- and mono-hydrated calcium oxalate including weddellite and whewellite since the unstable weddellite shows a trend to the stable whewellite. In that case, the crystal conversion still shows a mixture of weddellite and whewellite which can be determined by IR and microstructures.[19] Actually, related IR of such kidney stone while weddellite converts into whewellite, does not show the exact transition. Also, some subtle distinctives happen which illustrates an amorphous whewellite is formed during the dissolution-recrystallization process.

With regards to our work, the in-depth study of the crystal structures of cysteine and cystine, to understand better cystinosis has a major clinic interest as underlined by our recent investigation which points for the first time the presence of L-cysteine.[20] More precisely, the complete set of data seems to indicate that cystinosis is linked to the pathogenesis of cysteine crystallites associated with a rectangular morphology, and to the pathogenesis of cystine, as evidenced by our observation of hexagonal cystine crystals. So, a major question emerges: The drug of cystinosis has to avoid the pathogenesis of L-cystine crystals, the pathogenesis of L-cysteine crystals or the pathogenesis of both L-cysteine and L-cystine crystals?

In fact, cystine crystals normally consist of two cysteine crystal structure, but they have very different crystal properties in human body. Cystine ($[\text{-S-CH}_2\text{-CH-(NH}_2\text{)-COOH}]_2$) displays a hexagonal structure ($P6_122$ space group, $a = b = 5.412$ Å, $c = 55.956$ Å).[21] It's worth noting that the monoclinic L-cysteine ($C_3H_7NO_2S$) is shown by $a = 8.144$ Å, $b = 11.937$ Å and $c = 5.416$ Å with a space group $P2_1$.[22, 23] In order to characterize the crystalline structures at atomic level of cysteine and cystine, we combine First-Principles geometry optimization with

experimental methods including IR, XRD, Raman to explore the interaction between these two sorts of crystals.

2. Experimental details

2.1 The preparation of Cystine and Cysteine powders

Cystine (98%) and cysteine (≥ 98 %) powders were commercially acquired from Merck.

2.2 Measurements

XRD experiments were performed on the MORPHEUS experimental platform at the Laboratoire de Physique des Solides, Orsay, then carried out on a rotating anode (model RU H3R, Rigaku Corporation, Japan) using Cu Kα radiation (λ= 0.154 nm) delivered by a multilayer W/Si optics. Before detection, the powders filled borosilicate glass capillaries (1 mm diameter) and were measured by X-ray beam. Meanwhile, two-dimensional patterns were recorded on a MAR345 detector (marXperts GmbH, Germany) with 150 μm pixel size and a sample-detector distance of 150 mm. Extraction of the scattered intensity as a function of the 2θ scattering angle was performed through a home- developed software.

IR experiments on powder analysis were conducted according to the KBr pellet technique and the transmission mode. Infrared spectra were recorded on a Fourier transform infrared spectrophotometer Bruker IFS 25 (Japan) covering the range 2.5 - 25 μm (4000 - 400 cm^{-1}) implemented in Tenon Hospital. 32 scans were recorded for each spectrum at room temperature against air as reference.

2.3 Computational details

The Vienna Ab initio Simulation Package (VASP)[24, 25] has been used to perform all theoretical calculations. Periodic Density Functional Theory (DFT) was used to apply the augmented plane wave method (PAW)[26] to describe the electron-ion interactions with a cut-off energy of 500 eV.[27, 28] The functional of Perdew Burke Ernzerhof (PBE)[29] was employed, and the Kohn-Sham equations were solved self-consistently until the energy difference of the cycles was less than 10^{-8} eV. To improve total energy convergence, a Gaussian smearing with σ = 0.1 eV was applied to the band occupations. The atomic positions were fully optimized until all forces were smaller than 0.01 eV/Å per atom. To minimize computational cost, all calculations were performed only at the Γ-point. In order to take into account van der Waals interactions which were not included in the PBE functional,[30] the Grimme D3-correction method by introducing the Becke-Johnson damping potential.[31, 32]

The theoretical X-ray diffraction patterns of L-cystine and L-cysteine were carried out by the crystallographic calculations program using *FullProf* software[33] which referring the cell parameters obtained after geometrical structure optimized by DFT method. Moreover, the unit cell parameters of L-cystine and L-cysteine applied to perform simulations of XRD patterns were taken from Dahaoui et al.[21] and Moggach et al.,[26, 23] respectively.

The Density functional perturbation theory (DFPT) was employed to simulate the vibrational frequencies and intensities of IR,[34-36] using the relaxed structures for different adsorption modes investigated. In the dipolar approximation, the intensity of i_{th} normal mode of vibration at a frequency ω_i (**Eq. 1**), was proportional to the square of the change of dipole moment associated with the atomic motion along the eigenvector e_i of that mode:

$$I_i \propto \left|\frac{\partial P}{\partial R} ei\right|^2 = \sum_\alpha \left[\sum_l \sum_\beta Z_{\alpha\beta}(l) e_{i,\beta}(l)\right]^2 \qquad (1)$$

Where, $e_{i,\beta}(l)$ was displacement of i_{th}-atom in the eigenvector of the i_{th} normal mode and $Z_{\alpha\beta}(l) = \frac{\partial P\alpha}{\partial R\beta(l)}$ was the Born charge of the i_{th} atom, we obtained these quantities from the previous equations by employing the DFT implemented in VASP package.[24, 25]

Vibrational spectra have been calculated within the harmonic approximation. This matrix was computed by the finite difference method followed by a diagonalization procedure. The eigenvalues of the resulting matrix led to the frequency values. The assignment of the vibrational modes was done by inspection of the corresponding eigenvectors. The Raman intensities were then estimated by the derivative of the macroscopic dielectric tensor (polarizability) with respect to the normal mode, following the method of Fonari and Stauffer.[37]

It should be noted that L-cystine supersaturation was the main reason to form stone in cystinuria and cystinosis. To date, inhibitory factor for such L-cystine stone has not been found in urine. Furthermore, the solubility of L-cystine depends on the pH values in urine. The lower the pH value in urine is, the smaller the solubility is. L-cystine crystal do not dissolve under physiological environment (pH = 5.5 – 7.5), but they gradually dissolve while pH values are higher than 7.5. Therefore, we considered other conversion types about such crystals under normal physiological pH value. In this work, all calculations were conducted without taking into account the pH values.

3 Results

3.1 Geometrical parameters and energetics

The crystallographic information framework (CIF) of L-cysteine used to perform calculations of this work was taken from Moggach et al.[38] This CIF available on Crystallographic Open Database (COD) was registered with the number of 2009193. The unit cell contains four cysteine molecules in interaction via H-bonds forming double chains. The unit cell parameters of L-cysteine obtained after full relaxation (ISIF = 2) with DFT-D3-BJ level of theory were a = 7.532 Å, b = 12.647 Å, c= 5.437 Å. Compared to the work reported by Stephan et al,[22] the parameters have a small shift. The unit cell doubled in c-direction was represented in **Figure** .

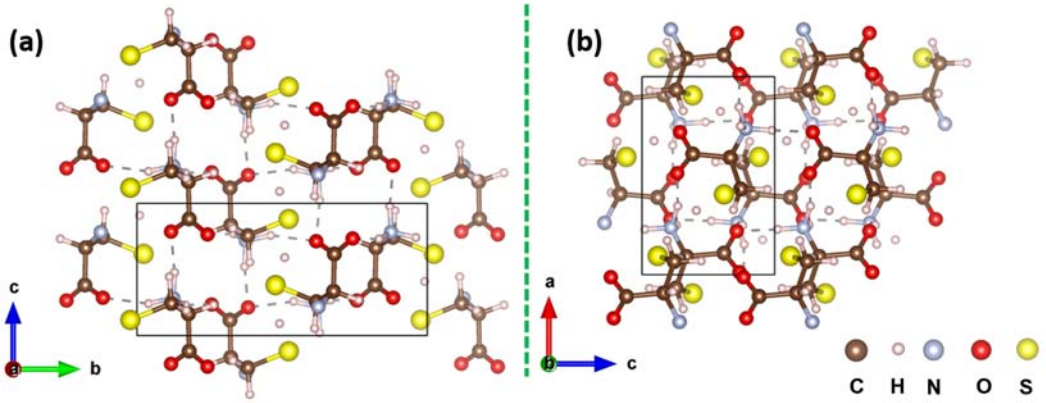

Figure 1. Unit cell of L-cysteine doubled in c-direction viewed from two directions (a) along a-axis; (b) along b-axis.

The L-cystine model used in this work was resolved by Dahaoui et al.[21] After optimizing at a DFT-level, the unit cell parameters have slightly changes with $a = b$ = 5.40390 Å, c = 56.3354 Å compared to the original crystal structure where $a = b$ = 5.42503 Å, c = 56.35397 Å. The unit cell doubled in a-direction was shown in **Figure 2**.

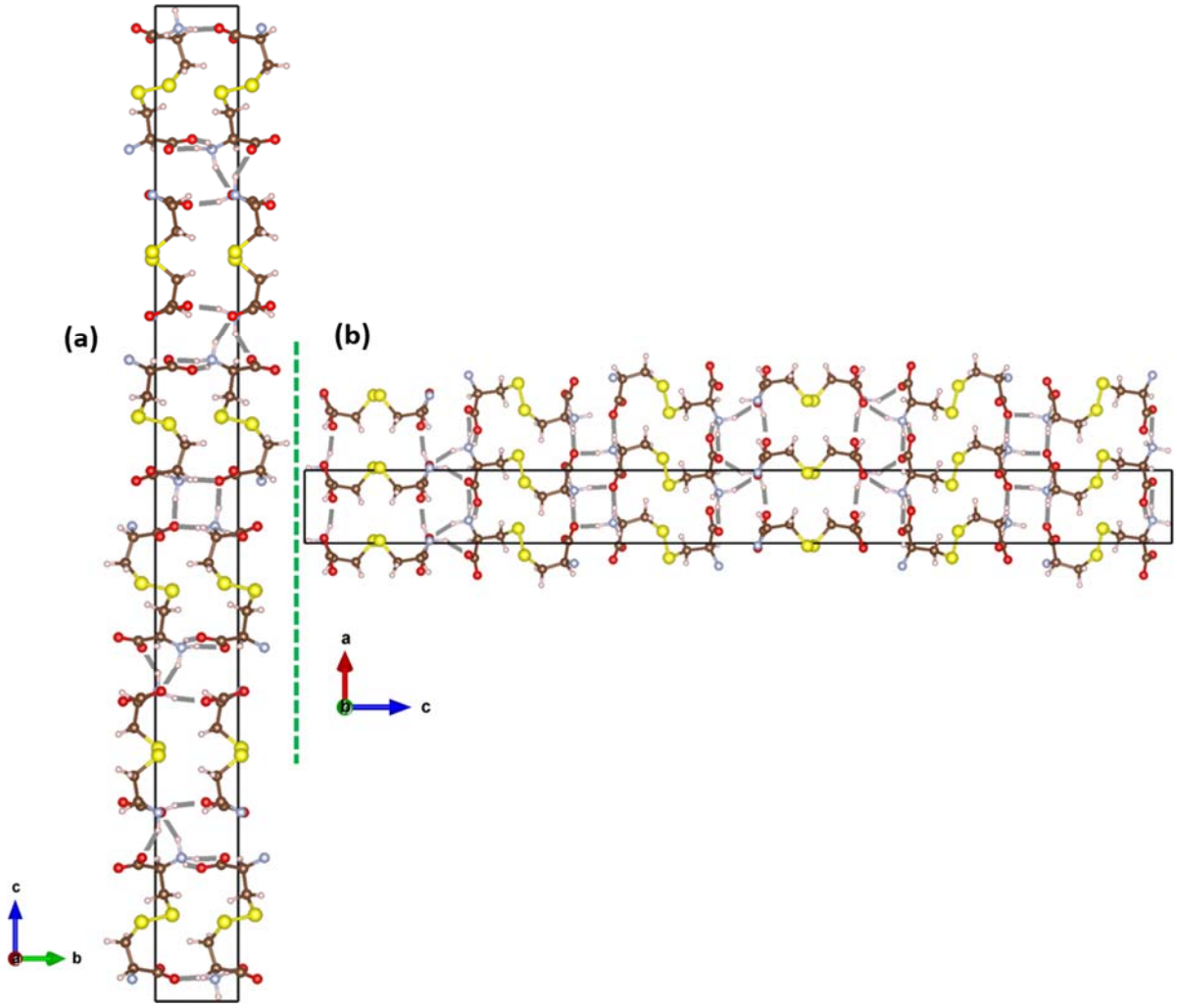

Figure 2. Unit cell of L-cystine doubled along *a*-direction viewed from two directions (a) along *a*-axis; (b) along *b*-axis.

L-cystine was obtained by dimerization of L-cysteine leading to the formation of a S-S bond between both L-cysteine fragments. The interatomic distances and bond angles obtained after full relaxation for L-cysteine and L-cystine were reported in **Table 1**. These geometric parameters vary very slightly regarding L-cysteine to that of L-cystine. The distance of calculated S-S bond between two cysteine fragments related to L-cystine crystal was 2.047 Å, while in the gas phase L-cystine molecule was 2.046 Å.

Table 1. Calculated interatomic distances and angles for L-cysteine and L-cystine (distances in Å and angles in°).

L-cysteine		L-cystine	
Distance		***Distance***	
C1-C2	1.528	C1-C2	1.540
C2-C3	1.535	C2-C3	1.525
C3-S	1.823	C3-S1	1.822
C2-N	1.485	S1-S2	2.047
S-H	1.365	S2-C4	1.822
C1-O1	1.276	C4-C5	1.525
C1-O2	1.261	C5-C6	1.540
		C2-N1	1.487
Angle		C5-N2	1.487
C1C2C3	111.4	C1-O1	1.281
C1C2N	111.1	C1-O2	1.258
C2C3S	114.9		
C3C2N	111.5	***Angle***	
C3SH	96.6	C1C2C3	113.2
NC2H	106.9	C1C2N1	110.4
		C2C3S1	117.3
Dihedral angle		S1S2C4	105.0
C1C2C3S	-120.9	S2C4C5	117.3
NC2C3S	70.7		
		Dihedral angle	
		C1C2C3S1	-68.8
		C2C3S1S2	79.0
		C3S1S2C4	76.2
		S1S2C4C5	79.0
		N1C2C3S1	57.7

The crystal binding energy of L-cysteine and L-cystine in this work was determined and reported in **Table 2**, which were -117.7 kJ/mol and -351.9 kJ/mol, respectively. With respect to L-cystine, Yang et al.[39] have reported a binding energy of -359.2 kJ/mol using COMPASS forcefield in BIOVIA's Materials Studio software which was very close to our calculated results. In addition, one can note that the binding energy of L-cystine was three times much higher than the binding energy of L-cysteine in absolute value. As L-cystine was a dimer of L-cysteine, one could expect that the binding energy of L-cystine should be about twice times than that of L-cysteine.

Table 2. Calculated binding energies (energies in kJ/mol).

	Binding energy (kJ/mol)
L-cysteine	-117.7
L-cystine	-351.9

3.2 XRD analysis

In order to distinguish the phase compositions of L-cystine and L-cysteine crystallites, XRD analysis obtained by calculation were carried out. **Figure 3A(a)** and **(b)** showed the experimental XRD data of the L-cystine in comparison with the simulated one. As can be seen, highly similar patterns were observed. The diffraction peaks of synthetic L-cystine could be successfully indexed in terms of the hexagonal structure with a space group of $P6_122$ which can be visible elsewhere.[15, 40] Meanwhile, the XRD patterns of synthetic and calculated L-cysteine were represented in **Figure 3B(a)** and **(b)**, respectively. The indexation of the experimental reflections lines was also consistent with the monoclinic system (space group $P2_1$), in good agreement with the plotted output from the DFT analyses. However, as you see there is a slight shift of the diffraction peaks of the calculated L-cystine and L-cysteine patterns regarding the experimental ones, toward higher 2θ.

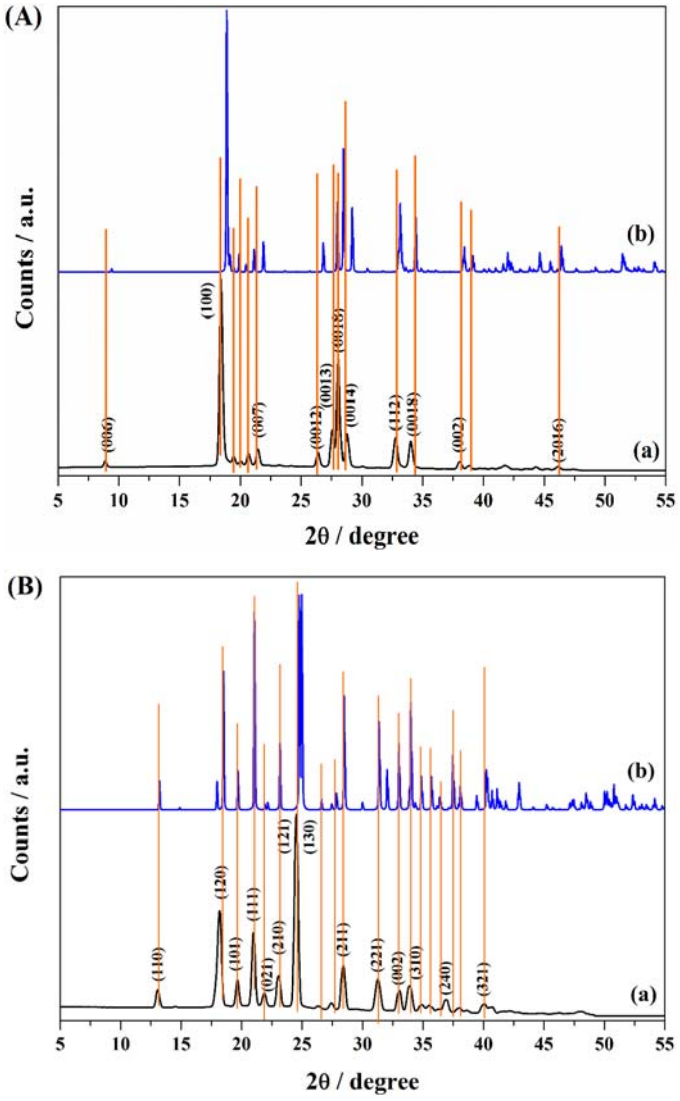

Figure 3. XRD patterns of L-cystine and L-cysteine, (A): experimental (a) and theoretical (b) results of L-cystine; (B): experimental (a) and theoretical (b) results of L-cysteine.

3.3 IR analysis

Regarding to S-H and S-S bend appearing in L-cysteine and L-cystine respectively (see **Figure 4a**), this fully illustrated the discrepancy between the theoretical results of L-cysteine and L-cystine. Experimental and theoretical IR spectra calculation of L-cysteine in the KBr phase in the frequency region 500 - 3500 cm^{-1} were similar and reported in **Figure 4(b)**. The assignments given in **Table 3** were in agreement with those given in the literature by Pawlukoj´c et al.[41] and Parker et al.[42] In **Figure 4(b)**, mainly regarding theoretical L-cysteine spectrum, the band at ~3068 cm^{-1} and ~2920 cm^{-1} were assigned to the CH_2 asymmetric stretch, which was in line with the range of ~3500 - ~2800 cm^{-1} in experimental IR spectrum.[42] The absorption peaks at ~2677 cm^{-1}, ~1583 cm^{-1}, ~1559 cm^{-1}, ~1351 $cm^{-1}$and ~1161 cm^{-1} belong to NH_3 asymmetric stretch.[41] The peaks obtained at ~1382 cm^{-1} and ~800 cm^{-1} were assigned at COO- asymmetric stretch. The bending vibrations of C-H occur at ~1295 cm^{-1}, ~1262 cm^{-1} and ~1083 cm^{-1}. The peaks at ~845 cm^{-1} and 568 cm^{-1} were due to the C-C bending vibrations. The characteristic bands at ~1010 cm^{-1} due to S-H bend. ~961 cm^{-1} and ~718 cm^{-1} represented characteristic of N-CH stretch and C-S stretch, respectively.[43] ~541 cm^{-1} was NH_3 torsion which can be seen in experimental stretch.[42] All these characteristic peaks well agreed with the experimental result.

Erreur ! Source du renvoi introuvable.**4(c)** showed the L-cystine's coincidently theoretical and experimental result, also detected between 500 - 3500 cm^{-1}, combined with **Table 4**, the appearance of ~1654 cm^{-1}, ~1639 cm^{-1}, ~1589 cm^{-1}, ~856 cm^{-1}, ~825 cm^{-1} and ~760 cm^{-1} adsorption peaks showed the NH_3 asymmetric bend.[43, 44] ~1507 cm^{-1} group confirmed the presence of stretching vibration of COO^-.[44] ~3042 cm^{-1}, ~1383 cm^{-1}, ~1323 cm^{-1}, ~1282 cm^{-1}, ~1238 cm^{-1} and ~1086 cm^{-1} adsorption bands were the stretching and bending vibrations of C-H.[45, 46] The ~1349 cm^{-1}, ~1161 cm^{-1} and ~1109 cm^{-1} peaks were generated by C-C stretching vibration.[43, 47] ~1036 cm^{-1} belonged to C-N stretching.[43] In addition, the peaks at ~532 cm^{-1} were marked in blue in the spectrum and assigned to the S-S stretch.[46] Noting that the bending stretch ~532 cm^{-1} appeared in both L-cysteine and L-cystine, but indicated different chemical groups.

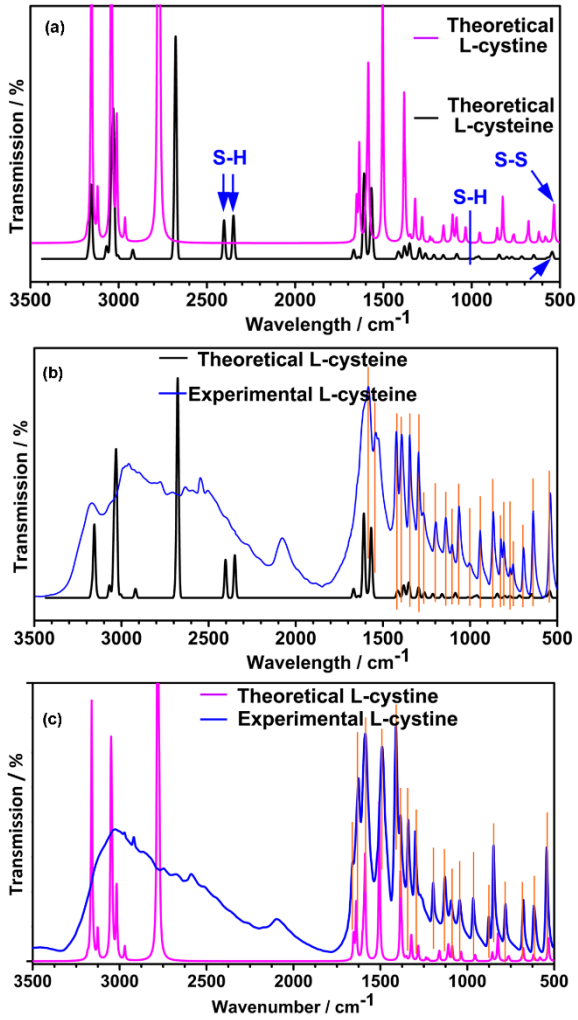

Figure 4. IR spectra of L-cysteine and L-cystine between 500 - 3500 cm^{-1}, (a) theoretical comparison of L-cysteine and L-cystine; (b) theoretical and experimental L-cysteine; (c) theoretical and experimental L-cystine.

Table 3. Theoretical and experimental IR comparisons of L-cysteine (values in cm^{-1}) and assignments.

Wavenumber (cm^{-1})		Assignment
Theoretical results	Experimental results	
3068, 2920	3500-2800	CH_2 asymmetric stretch
2677, 1583, 1559, 1351, 1161	2800-1600, 1586, 1541, 1346, 1137	NH_3 symmetric bend
1382, 800	1394, 803	COO-
1295, 1262, 1083	1296, 1268, 1063	C-H stretching
845, 568	867, 538	C-C stretching
2403, 2350, 1010	1003	SH bend
961	942	N-CH stretch
718	695	C-S stretch

541	538	NH_3 torsion

Table 4. Calculated and experimental IR comparisons of L-cystine (values in cm^{-1}) and assignments.

Wavenumber (cm^{-1})		Assignment
Theoretical results	Experimental results	
3042	3500-2800	CH_2-S asymmetric stretch
2785, 1654, 1639, 1589, 856, 825, 760	2800-1700, 1656, 1622, 1584, 872, 845, 778	NH_3 asymmetric bend
1507	1485	COO-
1349, 1161, 1109	1372, 1197, 1125	C-C stretching
1383, 1323, 1282, 1238, 1086	1338, 1295, 1263, 1091	CH stretching
1036	1035	C-N stretching
532	538	S-S stretch

3.4 Raman analysis

Raman spectra of the L-cysteine and L-cystine were calculated using DFT method. Different molecular vibrations were shown in **Figure 5** and referred vibrations regarding the experiments completed by other researchers, listed in **Table 5**, which can also help to distinguish the discrepancy of the L-cysteine and L-cystine. Apparently, similar to above IR results, the peaks at ~2452 cm^{-1}, ~2407 cm^{-1}, ~942 cm^{-1}, ~858 cm^{-1}, ~798 cm^{-1}, ~764 cm^{-1} and ~528 cm^{-1} corresponded to the S-H group stretching frequency which did not generate in L-cysteine's Raman spectrum. In comparison, a peak at ~470 cm^{-1} appeared according to the Raman plotting of L-cystine, which was associated to the S-S bond. More specifically, other bands and related stretches can be found in **Table 5**.

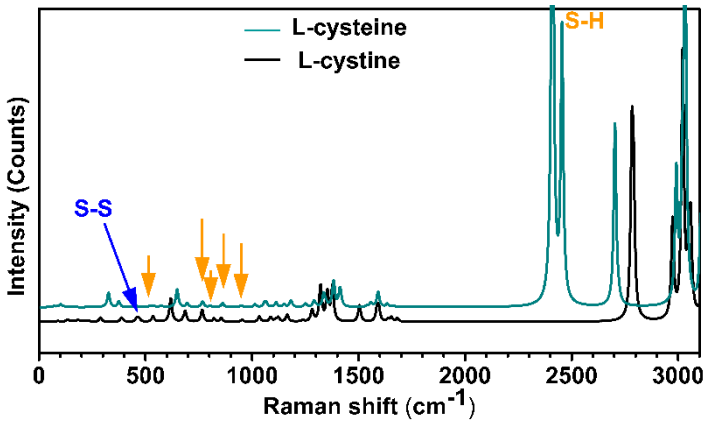

Figure 5. Theoretical Raman spectrum of L-cysteine and L-cystine.

Table 5. Calculated Raman modes wavenumbers (in cm^{-1}) and assignment with the type of vibration.

L-cysteine

Present theoretical band	Assignment	Assignment Literature
3028	CH stretch	
2987	NH stretch	[46]~3040 NH stretch
2700	O-H	[46]~2950
2452		[46]~2554
2407	SH stretch	[38]~2350, 2545
1661		~1300 - ~1700, CH_2 bend, COO- stretch, NH_3 bend.
1631	CO_2 asymmetric stretch NH_3^+ bend	[38]~1633 NH_3 bend asymmetric; ~1662 CO_2 asymmetric stretch
1589		
	NH_3^+ bend	
1555	NH_3^+ bend	
1410	CH_2 bend	
1380	CO_2symmetric stretch CH_2 bend	
1334 1289	CH_2 bend NH_2 rock	
1248	CH_2 wag NH_3 rock	between ~1000 - ~1300 signals of SH bend, CH_2 twist, CH_2 wag, CH bend
1179	CH_2 twist NH_3 rock	~1180 CH_2 twist ~1200 CH_2 twist ~1107 - ~1162 NH_3 rock
1146	CH_2 wag NH_3 rock	~1107 - ~1162 NH_3 rock ~1180 CH_2 twist ~1200 CH_2 twist
1140	CH_2 twist NH_3 rock	~1107 - ~1162 NH_3 rock
1058	CN stretch CH_2 twist	[47]~1083 C-N stretch
1010	CH_2 -CH stretch	~999 CH_2-CH stretch; ~600 - ~1000 are observed C-S, C-C link vibrations. also bending vibrations of COO-
942	SH bend CH_2 rock	~961 - ~987 S-H in-plane bend
858	CH_2 bend SH bend C-CO_2 stretch	~918 C-CO_2-stretch

798	SH bend CO_2symmetric bend	~600 - ~1000 CO_2 bend
764	SH bend CH_2 bend	
692	C-S stretch	~692 C-S stretch
644	C-S stretch	~662, ~680 C-S stretch
570	lattice vibrations	~200 - ~600, vibrations of CCC, CCS, CCN
528	SH bend CH_2 bend	~346 - ~439 S-H out-of-plane bend
445 370	CCN bend	~469 CCN bend
322	CCN bend CH_2 rock	~300 CCN bend
232	lattice vibrations	~200 - ~50 lattice vibrations
98 65	lattice vibrations	

L-cystine

Present theoretical band	Assignment	Assignment Literature
3024	NH stretch CH stretch	
2977	CH stretch	~2967 ~2966 and ~2912
2783	NH stretch	
1685	NH_2 asymmetric bend	
1655	NH_2 asymmetric bend	~1611 NH_2 bend
1584	NH_2 bend COO- asymmetric stretch	
1508	NH_3 wag	
1378	CH_2 bend COO- symmetric bend	~1407 COO- symmetric stretch. ~1384 CH bend
1355	CH_2 bend COO- symmetric bend	
1323	CH bend COO- symmetric bend	
1289	CH_2 twist	

1166	CH_2 twist CH bend	
1124	CH_2 twist NH_3 rock	
1035	CH_2 twist	
1028	CH_2 twist	
956	CH_2-CH stretch NH_3 rock	
856	CH_2 rock NH_2 rock	
822	CH_2 rock	
767	CH_2 rock HCN bend	
676	C-S stretch CH_2 wag NH_2 rock	~677 C-S stretch
614	C-S stretch CH_2 rock NH_3 torsion	
540	CH_2-CH-N bend	
470	S-S stretching	~498 S-S stretch
455	CH_2-CH-N bend	
387	CH_2-CH-N bend	
293	CH_2-CH-N bend CH_2 rock	
250 - 0	Lattice vibrations	

4 Discussion

Figure 1 and 2 were the configurations of L-cysteine and L-cystine. The changes of related unit cell parameters occurred during the optimization, but the result was in agreement with the experimental values according to the X-ray result,[15] which can provide more accurate configurations for the latter calculations. In terms of the distance of S-S bond, the calculated one was a little less than the general length (~2.05 Å). The stretching of the S-S bond observed in the crystal may be due to the hydrogen bond interactions undergone from the neighboring L-cystine molecules. Indeed, the S-S bond was a center of symmetry in the L-cystine molecule. Thus, the interactions acted simultaneously on both groups located on both sides of the S atoms of L-cystine, causing the stretching of the S-S bond. This difference can be explained by the possibility of the isolated L-cystine molecule to reorganize itself and reach a much more stable

configuration. In fact, L-cystine was present in its ionic form (-CH(NH_3^+)-COO^-) which was rearranged when it was isolated (-CH(NH_2)-COOH). But the rearrangement did not occur in the case of isolated L-cysteine. This can be concluded that the energetic difference occurred between L-cystine and double L-cysteine molecules, indicating that the L-cysteine crystal was more stable than that of L-cystine crystal.

Based on this, the phase composition of these two types of crystals was deeply studied as well combined with XRD, IR and Raman spectrum. For the XRD analysis, the difference between the experimental and theoretical results may be caused due to the DFT-D3 correction method. It took into account the van der Waals interactions, thus leading to a slight change in the calculated unit cell parameters with regards to L-cystine and L-cysteine. Collectively, the experimental XRD results showed the phase compositions of L-cystine and L-cysteine which were well verified by DFT methods according to specific molecular modellings. In order to further analyze the chemical groups in L-cystine and L-cysteine, IR spectra were studied as shown in **Figure 4**. In contrast, as seen from **Figure 4(a)**, the differences mainly appeared on S-H bend (only formed in L-cysteine) and S-S stretch (only found in L-cystine), which connected double L-cysteine and formed L-cystine crystal) between L-cystine and L-cysteine crystals. Apparently, according to **Figure 4(b, c)**, small shift led to discrepancy between theoretical and experimental IR results of L-cysteine and L-cystine. This can be interpreted by the presence of van der Waals interactions. More specifically, the calculations in this work were carried out at 0 K, but the experiments were performed at around 300 K which more or less affected the spectrum detection. Additionally, the small shifts related to the experimental and theoretical results of L-cysteine and L-cystine may also be caused by the pressure in the reaction context. Therefore, these aspects negatively impacted the harmonic oscillator approximation. The theoretical results regarding the L-cysteine and L-cystine were well agreed with the experimental ones, which inferred the chemical components appeared in both types of crystals. Also, it indicated that the difference happened between crystals we studied, connected by the S-S bond. In order to further prove the difference about the S-H and S-S bonds, the theoretical Raman result obtained for L-cystine and L-cysteine were found to be in good agreement with the experimental ones reported by Michal Ejgenberg, Yitzhak Mastai and Rimer.[15, 17] As we mentioned before, Raman results can well display the S-H and S-S stretches with respect to the different sorts of crystals. This can provide clear conception for distinguishing the existence and relationship of the L-cystine and L-cysteine.

From the molecular view and chemical characterizations of the L-cystine and L-cysteine, we can understand their relationship deeply in order to study how L-cystine divided

into two L-cysteine. Today, drugs carrying SH groups are commonly used, such as cysteamine for the treatment of cystinosis or d-penicillamine and mercaptoporpionylglycine for the treatment of cystinuria. Thereby, our experimental and theoretical data could be of interest to develop new treatments for cystinuria and cystinosis.

5 Conclusion

L-cystine, as a urinary stone component in pathological cystinuria and as cells deposits in cystinosis was associated with L-cysteine only in cystinosis. In our work, the interaction between L-cysteine and L-cystine were analyzed by combining theoretical and experimental methods. Especially IR spectra and Raman spectra systematically illustrated the presence of functional groups of these two matters which can be apparently distinguished by the S-S bond. The XRD result apparently confirmed the structural identity of the L-cystine and L-cysteine crystallites. It is probably assumed that L-cystine crystals related to cystinuria and cystinosis as well result from the conversion of L-cysteine. Then a phase transition can occur in cystinosis disease resulting in a mixing of L-cysteine and L-cystine.

6 Acknowledgements

Computational resources and services were also provided by the Shared ICT Services Centre funded by the Vrije Universiteit Brussel, the Flemish Supercomputer Center (VSC) and FWO. ET wishes to thank the VUB for a Global Minds. YS wishes to thank for a China Scholarship Council (CSC) grant for performing her research at the VUB. FT wishes to acknowledge the VUB for support, among other through a Strategic Research Program awarded to his group.

7 Disclosure of potential conflicts of interest

The authors declare no potential conflict of interest

8 Research involving Human Participants and/or Animals

The research presented in this article does not involve human Participants and/or Animals

9 Informed consent

Not applicable since no human participant has been involved in the presented study

10 References

[1] Tasian, G. E.; Jemielita, T.; Gsoldfarb, D. S.; Copelovitch, L.; Gerber, J. S.; Wu, Q.; Denburg, M. R., Oral Antibiotic Exposure and Kidney Stone Disease. Journal of the American Society of Nephrology 2018, ASN.2017111213.

[2] Bazin, D.; Bouderlique, E.; Daudon, M.; Frochot, V.; Haymann, J. P.; Letavernier, E.; Tielens, F.; Weil, R., Scanning electron microscopy-a powerful imaging technique for the clinician. Comptes Rendus. Chimie 2021, 24 (S2), 1-24.

[3] Abbagani, S.; Gundimeda, S. D.; Varre, S.; Ponnala, D.; Mundluru, H. P., Kidney stone disease: Etiology and evaluation. International Journal of Applied Biology and Pharmaceutical Technology 2010, 1 (1), 175-182.

[4] Sivaguru, M.; Saw, J. J.; Wilson, E. M.; Lieske, J. C.; Krambeck, A. E.; Williams, J. C.; Romero, M. F.; Fouke, K. W.; Curtis, M. W.; Kear-Scott, J. L., Human kidney stones: a natural record of universal biomineralization. Nature Reviews Urology 2021, 1-29.

[5] Elmonem, M.A.; Veys, K.R.; Soliman, N.A.; van Dyck, M.; van den Heuvel, L.P.; Levtchenko, E., Cystinosis: a review. Orphanet journal of rare diseases 2016, 11 (1), 1-17.

[6] Romero, V.; Akpinar, H.; Assimos, D. G., Kidney stones: a global picture of prevalence, incidence, and associated risk factors. Reviews in Urology 2010, 12 (2-3), e86.

[7] Bazin, D.; Frochot, V.; Haymann, J. P.; Letavernier, E.; Daudon, M., Crystal size in μ crystalline pathologies and its clinical implication. Comptes Rendus. Chimie 2021, 24 (S2), 1-15.

[8] Tielens, F.; Vekeman, J.; Bazin, D.; Daudon, M., Opportunities given by density functional theory in pathological calcifications. Comptes Rendus. Chimie 2021, 24 (S2), 1-10.

[9] Dahlberg, P. J.; Berg, V. D.; Kurtz, S. B.; Wilson, D.M.; Smith, L. H., Clinical features and management of cystinuria. Mayo Clinic Proceedings 1977, 52 (9), 533.

[10] Koulivand, L.; Mohammadi, M.; Ezatpour, B.; Salehi, R.; Markazi, S.; Dashti, S.; Kheirollahi, M., Mutation analysis of SLC3A1 and SLC7A9 genes in patients with cystinuria. Urolithiasis 2015, 43 (5), 447-453.
[11] Andreassen, K. H.; Predersen, K. V.; Osther, S. S.; Jung, H. U.; Lildal, S. K.; Osther, P. J. S., How should patients with cystine stone disease be evaluated and treated in the twenty-first century? Urolithiasis 2016, 44 (1), 65-76.
[12] Lee, M. H.; Sahota, A.; Ward, M.; Goldfarb, D. S., Cystine Growth Inhibition Through Molecular Mimicry: a New Paradigm for the Prevention of Crystal Diseases. Current Rheumatology Reports 2015, 17 (5), 33.
[13] Prot-Bertoye, C.; Lebbah, S.; Daudon, M.; Tostivint, I.; Bataille, P.; Bridoux, F.; Brignon, P.; Choquenet, C.; Cochat, P.; Combe, C., CKD and its risk factors among patients with cystinuria. Clinical Journal of the American Society of Nephrology 2015, *10* (5), 842-851.
[14] Bazin, D.; Daudon, M.; André, G.; Weil, R.; Véron, E.; Matzen, G., Therapy modifies cystine kidney stones at the macroscopic scale. Do such alterations exist at the mesoscopic and nanometre scale? Journal of Applied Crystallography 2014, 47 (2), 719-725.
[15] Rimer, J. D.; An, Z.; Zhu, Z.; Lee, M. H.; Gol Df Arb, D. S.; Wesson, J. A.; Ward, M., Crystal growth inhibitors for the prevention of L-cystine kidney stones through molecular design. Science 2010, 330 (6002), 337-341.
[16] Mitchell; J. S., Progress in Radiobiology. Progress in radiobiology: 1956.
[17] Ejgenberg, M.; Mastai, Y., Biomimetic Crystallization of l-Cystine Hierarchical Structures. Crystal Growth & Design 2012, 12 (10), 4995–5001.
[18] Dewey, D. L.; Beecher, J., Interconversion of Cystine and Cysteine induced by X-rays. Nature 1965, 206 (991), 1369-1370.
[19] Bazin, D.; Leroy, C.; Tielens, F.; Bonhomme, C.; Bonhomme-Coury, L.; Damay, F.; Denmat, D. L.; Sadoine, J.; Rode, J.; Frochot, V., Hyperoxaluria is related to whewellite and hypercalciuria to weddellite: What happens when crystalline conversion occurs? Comptes Rendus Chimie 2016, 19 (11–12), 1492-1503.
[20] Wilmer, M.J.; Schoeber, J.P.; van den Heuvel, L.P.; Levtchenko, E.N., Cystinosis: practical tools for diagnosis and treatment. Pediatric nephrology 2011, *26* (2), 205-215.
[21] Dahaoui, S.; Pichon-Pesme, V.; Howard, J.; Lecomte, C., CCD charge density study on crystals with large unit cell parameters: The case of hexagonal L-cystine. The Journal of Physical Chemistry A 1999, 103 (31), 6240-6250.
[22] Moggach, S. A.; Clark, S. J.; Parsons, S., l□Cysteine□I at 30 K. Acta Crystallographica Section E 2005, 61 (8), o2739-o2742.
[23] Allan, D. R.; Clark, S. J.; Gutmann, M. J.; Sawyer, L.; Moggach, S. A.; Parsons, S.; Pulham, C. R., High-pressure polymorphism in L-cysteine: the crystal structures of L-cysteine-III and L-cysteine-IV. Acta Crystallographica 2010, 62 (2), 296-309.
[24] Kresse, G.; Furthmüller, J., Vienna ab-initio simulation package (VASP). Vienna: Vienna University 2001.
[25] Kresse, G. G.; Furthmüller, J. J., Efficient Iterative Schemes for Ab Initio Total-Energy Calculations Using a Plane-Wave Basis Set. Physical review. B, Condensed matter 1996, 54, 11169.
[26] Kresse, G.; Hafner, J., Norm-conserving and ultrasoft pseudopotentials for first-row and transition elements. Journal of Physics: Condensed Matter 1994, 6 (40), 8245.
[27] Kulkarni, B. S.; Krishnamurty, S.; Pal, S., Influence of plane wave cut-off on structural and electronic properties in Sn-BEA and Ti-BEA zeolite water molecule interaction. Chemical Physics Letters 2010, 484 (4-6), 374-379.
[28] Lapere, K. M.; Lamacchia, R. J.; Quak, L. H.; Mckinley, A. J.; Wild, D. A., Anion photoelectron spectroscopy and ab initio calculations of the gas phase chloride-carbon monoxide complex: ClCO. Chemical Physics Letters 2011, 504 (1-3), 13-19.
[29] Perdew, J. P.; Burke, K.; Ernzerhof, M., Generalized Gradient Approximation Made Simple. Physical Review Letters 1996, 77 (18), 3865.
[30] Chibani, S.; Chebbi, M.; Lebègue, S.; Bučko, T.; Badawi, M., A DFT investigation of the adsorption of iodine compounds and water in H-, Na-, Ag-, and Cu-mordenite. The Journal of chemical physics 2016, 144 (24), 244705.

[31] Ehrlich, S.; Moellmann, J.; Reckien, W.; Bredow, T.; Grimme, S., System-Dependent Dispersion Coefficients for the DFT-D3 Treatment of Adsorption Processes on Ionic Surfaces. Chemphyschem 2011, 12 (17), 3414-3420.
[32] Grimme, S.; Ehrlich, S.; Goerigk, L., Effect of the damping function in dispersion corrected density functional theory. Journal of Computational Chemistry 2011, 32 (7), 1456-1465.
[33] Rodríguezcarvajal, J., An Introduction to the Program FullProf 2000. 2001.
[34] Hutter, J.; Luethi, H. P.; Diederich, F., Structures and vibrational frequencies of the carbon molecules C2-C18 calculated by density functional theory. Journal of the American Chemical Society 1994, 116 (2), 750-756.
[35] Karhanek, D., Self-assembled monolayers studied by density-functional theory. Doctoral dissertation, Uniwien, 2010.
[36] Karhánek, D.; BučKo, T.; Hafner, J., A density functional study of the adsorption of methanethiol on the (111) surfaces of the Ni-group metals: I. Molecular and dissociative adsorption. Journal of Physics Condensed Matter An Institute of Physics Journal 2010, 22 (26), 265006.
[37] Fonari, A.; Stauffer, S., vasp_raman.py. https://github.com/raman-sc/VASP/: 2013.
[38] Moggach, S. A.; Allan, D. R.; Clark, S. J.; Gutmann, M. J.; Parsons, S.; Pulham, C. R.; Sawyer, L., High-pressure polymorphism in L-cysteine: the crystal structures of L-cysteine-III and L-cysteine-IV. Acta Crystallogr B 2006, 62 (Pt 2), 296-309.
[39] Hu, L. Q.; Yang, Y. H.; Aloysius, H.; Albanyan, H.; Yang, M.; Liang, J. J.; Yu, A.; Shtukenberg, A.; Poloni, L. N.; Kholodovych, V.; Tischfield, J. A.; Goldfarb, D. S.; Ward, M. D.; Sahota, A., l-Cystine Diamides as l-Cystine Crystallization Inhibitors for Cystinuria. Bioorganic & Medicinal Chemistry Letters 2018, 59 (8), 1303-1308.
[40] Iordanidis, A.; Garcia-Guinea, J.; Correcher, V.; Goundas, I., Optical and Spectral Observations on Cystine, Oxalate, and Apatite Renal Calculi. Spectroscopy Letters 2011, 44 (7-8), 490-494.
[41] Pawlukoj, A.; Leciejewicz, J.; Ramirez-Cuesta, A. J.; Nowicka-Scheibe, J., L-Cysteine: Neutron spectroscopy, Raman, IR and ab initio study. Spectrochimica Acta Part A Molecular & Biomolecular Spectroscopy 2005, 61 (11-12), 2474-2481.
[42] Parker, S. F., Assignment of the vibrational spectrum of l-cysteine. Chemical Physics 2013, 424 (424), 75-79.
[43] Ramachandran, E.; Natarajan, S., Crystal growth of some urinary stone constituents: III. In□ vitro crystallization of L□cystine and its characterization. Crystal Research & Technology 2010, 39 (4), 308-312.
[44] Pandey, C. M.; Sumana, G.; Malhotra, B. D., Microstructured cystine dendrites-based impedimetric sensor for nucleic acid detection. Biomacromolecules 2011, 12 (8), 2925.
[45] Ramachandran, E.; Natarajan, S., Crystal growth of some urinary stone constituents: III. In-vitro crystallization of L-cystine and its characterization. Crystal Research and Technology 2004, 39 (4), 308-312.
[46] Girija, E. K.; Kalkura, S. N.; Ramasamy, P., Crystallization of cystine. Journal of Materials Science Materials in Medicine 1995, 6 (11), 617-619.
[47] Estepa, L.; Daudon, M., Contribution of Fourier transform infrared spectroscopy to the identification of urinary stones and kidney crystal deposits. Biospectroscopy 1997, 3 (5), 347-369.

Data Availability

All data used in this research are available to the readers upon request.

TOC Figure